TEM Imaging of Polymer Multilayer Particles: Advantages, Limitations, and Artifacts

Zhixiang Wei,[†] Ilya Gourevich,[†] Lora Field,[†] Neil Coombs,[†] and Eugenia Kumacheva*[,†,‡,§]

Department of Chemistry, University of Toronto, 80 St. George Street, Toronto, Ontario M5S 3H6, Canada; Department of Chemical Engineering and Applied Chemistry, University of Toronto, 200 College Street, Toronto, Ontario M5S 3E5, Canada; and Institute of Biomaterials & Biomedical Engineering, University of Toronto, 4 Taddle Creek Road, Toronto, Ontario M5S 3G9, Canada

Received September 18, 2005
Revised Manuscript Received October 27, 2005

Core−shell polymer latex particles are intensively used in paints, coatings, adhesives, and impact modifiers.[1,2] Recently, several applications of core−shell and multilayer particles in "high-tech" applications emerged such as the production of materials for three-dimensional optical data storage,[3] security data encryption,[4] multilayer dielectric resonators,[5] and photonic crystals.[6]

Submicrometer-size core−shell and multilayer latex particles are typically obtained by interfacial emulsion polymerization in which the shell-forming polymer is polymerized on the surface of seeded "core" particles.[7−9] The synthesis of latex particles with a core−shell morphology is a desirable but not the sole scenario of such synthesis: raspberry, acorn, sandwich, and even phase-inverted core−shell particles have been reported.[10] The formation of a particular structure of microbeads is governed by the interplay of thermodynamic and kinetic factors such as the interfacial energy between the constituent polymers, the type of initiator used, the feeding rate of monomers, the degree of cross-linking of the polymers, and the reaction temperature.[7−10]

The multiphase structure of the composite latex particles is typically characterized by transmission electronic microscopy (TEM),[7−10] atomic force microscopy (AFM),[11] confocal fluorescent microscopy (CFM),[4,12] scanning transmission X-ray microscopy (STXM),[13] solid-state nuclear magnetic resonance (NMR) spectroscopy,[14] and differential scanning calorimetry (DSC).[15] Sundberg et al.[16] combined SEM, TEM, DSC, and NMR methods to determine the structure of core−shell latex particles. Among these methods, imaging the structure of particles by using TEM is the most straightforward method, especially when energy-dispersive X-ray (EDX) detectors are available for elemental analysis of different phases.

Herein we report advantages, limitations, and artifacts of TEM imaging of multilayer polymer particles. The microbeads were synthesized in a semicontinuous emulsion polymerization process in which styrene and trifluoroethyl methacrylate were supplied to the reaction mixture in five alternating stages. The recipe for the synthesis of the particles was reported elsewhere.[5c] It was assumed that in the resulting particles polystyrene (PS) and poly(trifluoroethyl methacrylate) (PTFEMA) will form a PS core and four alternating layers with high ($n = 1.59$) and low ($n = 1.43$) refractive indices,[17] respectively. Such structure was inspired by the potential use of PS−PTFEMA particles as the multilayer dielectric resonators.[5]

Scanning electron microscopy (SEM, S-5200, Hitachi) was employed to examine particle size and shape. A scanning transmission electron microscope (STEM, HD-2000, Hitachi) was used to characterize the internal structure of the multilayer particles. The difference in densities of PTFEMA and PS (1.45 and 1.06 g/cm^3, respectively[17,18]) made it possible to observe the multilayer structures by TEM, whose contrast is correlated to the mass−thickness of the specimen.[19] The detectors of STEM included a secondary electron detector (SE images) and two transmission electron detectors for bright field imaging (BF-STEM) and for high angle annular dark field imaging (HAADF-STEM). An energy-dispersive X-ray (EDX) spectrometer was coupled with the STEM instrument. Imaging experiments were conducted in several modes: we imaged intact individual microbeads and examined the structure of 70 nm thick particle slices. The slices were obtained in two ways. In the first method, we dispersed the microbeads in a 10% aqueous glycerol solution, froze the dispersion in liquid nitrogen at −196 °C, and then cryomicrotomed the particles with a glass knife (Leica Ultracut UCT microtome in a cryochamber) at −160 °C. Alternatively, we embedded the microbeads in epoxy resin (#052, low-viscosity resin kit, Canemco Inc., standard recipe) and microtomed them at room temperature.

Examination of Particle Morphology in Different Modes. Figure 1 shows the morphology of the PS−PTFEMA multilayer particles examined by using SEM and STEM. To achieve better contrast, during TEM imaging we used a HAADF detector. In such experiments contrast between the different phases of the sample depends on the atomic numbers of elements comprising these phases and the density of phases.

Figure 1a shows representative images of the cryomicrotomed multilayer beads. In each particle a polystyrene core and the two PS layers appeared dark and two PTFEMA layers appeared bright, consistent with the order of feeding styrene and trifluoroethyl methacrylate in the reaction mixture. Periodic modulation in the brightness of the layers confirmed a multilayer morphology of the microspheres. We note that in Figure 1a the particles did not appear spherical while the SEM image in Figure 1d confirmed their spherical shape. Similar distortion in the shape of cryomicrotomed spherical latex microbeads was observed by several groups.[10] The reason for the distortion in particle shape could originate from the shear force applied to the microbeads.

Figure 1b shows a representative TEM image of the multilayer microspheres embedded in epoxy resin and microtomed at room temperature. Two features contrast this image from Figure 1a: (a) the particles largely retain their spherical shape due to the "support" of the hard epoxy resin during microtoming, and (b) the particles feature a dark PS core and three (instead of four) consecutive layers of PTFEMA, PS, and PTFEMA. The forth PS layer is barely observed due to the low density contrast with the matrix of epoxy resin.

We also found that at an accelerating voltage of 200 kV particle morphology could be examined by the "imaging through" method which did not require the microtoming of the sample. Since STEM is free of post-specimen lenses, the chromatic aberrations were significantly reduced, and consequently, in the dark field mode imaging of samples with the

[†] Department of Chemistry.
[‡] Department of Chemical Engineering and Applied Chemistry.
[§] Institute of Biomaterials & Biomedical Engineering.
* Corresponding author. E-mail: ekumache@chem.utoronto.ca.

10.1021/ma052029z CCC: $33.50
Published on Web 03/14/2006

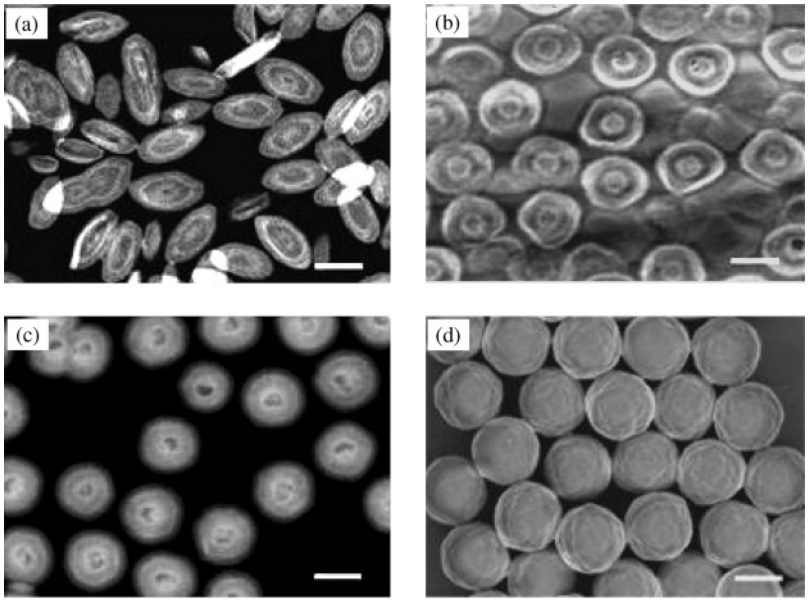

Figure 1. (a) HAADF-STEM images of microbead slices obtained by cryomicrotoming. (b) HAADF-STEM images of slices obtained by microtoming the particles embedded in epoxy resin at room temperature. In (a, b) the thickness of the slices is 70 nm. (c) HAADF-STEM images of intact particles obtained by "imaging through" the microbeads. The accelerating voltage and emission current are 200 kV and 30 μA, respectively, for all the STEM images. (d) Typical SEM images of the four-layer particles with a PS core and alternating layers of PTFEMA and PS. Scale bars are 1 μm.

thickness of up to 2 μm was possible.[20] In these experiments a droplet of latex emulsion was deposited on the TEM grid and allowed for evaporation of water. Figure 1c shows a typical dark field TEM image of the multilayer particles with the same sequence of alternating dark and bright layers and the relationship between their thicknesses as in Figure 1a,b. We admit however that in Figure 1c the interface between the PS and PTFEMA layers in not as sharp as in the images of microtomed particles. The blurriness of the interfaces was attributed to the interference of neighboring layers in the nonmicrotomed particles along the pathway of the electron beam. Nevertheless, this relatively simple "express" method could be successfully used for the qualitative examination of the multilayer morphology of microbeads.

"Contrast Inversion" Induced by Irradiation. For the cryomicrotomed particles, we routinely observed contrast inversion during imaging under magnifications above 15 000×. Figure 2 shows typical TEM and SE images of the four-layer particles cryomicrotomed at −160 °C and imaged under magnification 60 000× by using a 200 kV electron beam. Originally, the PS core and the PS layers appeared dark, and PTFEMA layers were light. Contrast inversion occurred in several seconds after the beginning of imaging (Figure 2a). In addition, following irradiation a smooth surface of the slice became rough (Figure 2b). The effect of contrast inversion occurred due to the stronger etching of the PTFEMA phase. Fluorinated polymers are radiation degradable: chain scission, cross-linking of polymer chains, and the overall loss of polymer mass occur under irradiation with an electron beam.[21] We conclude that examination of particle morphology under high magnification can be misleading unless special care is taken to reduce contrast inversion.

To minimize radiation-induced damage of the specimen, we carried out cryoSTEM imaging, in which the temperature of the sample holder during imaging was maintained at −100 °C. Figure 3a,b shows typical TEM micrographs of the microtomed particles imaged under different magnification. The quality of the TEM image of the collection of particles (Figure 3a) dramatically improved in comparison with Figure 1b. In Figure 3b a high-magnification TEM image provided the most detailed information about the composition and structure of the multilayer particles. This image showed the effect of the order of polymerization of styrene and trifluoroethyl methacrylate on the sharpness of interfaces in the latex microsphere. When PS was synthesized on the surface of the PTFEMA layer, the interface was sharper than that when PTFEMA was synthesized on the PS layer. Moreover, a high-resolution TEM image in Figure 3b allowed us to analyze the multiphase structure of the latex beads quantitatively. For instance, for the first and second layers of the particle in Figure 3b we estimated the thicknesses of the

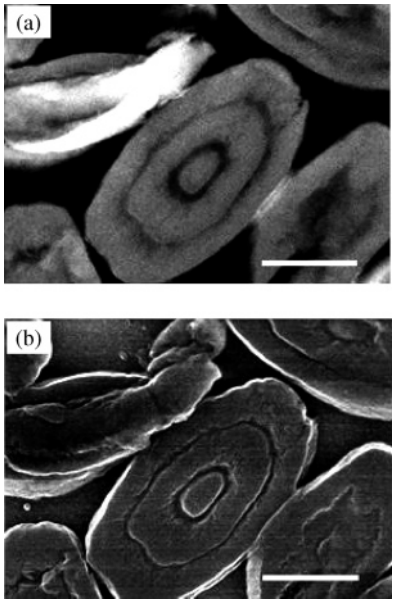

Figure 2. (a) HAADF-STEM image of the cryomicrotomed multilayer particle slice obtained at magnification 60 000×. This image shows "contrast inversion" comparing with the image acquired for the same sample at magnification 7000× in Figure 1a. (b) SE image of the same slice obtained at magnification 60 000×. The appearance of surface roughness in this image indicates that the PTFEMA phase is etched. The accelerating voltage and emission current were 200 kV and 30 μA, respectively. Scale bars are 500 nm.

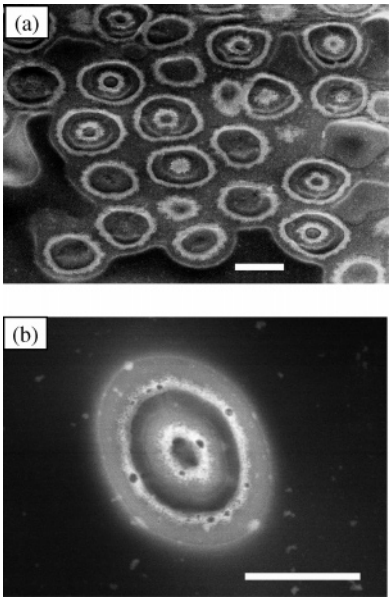

Figure 3. Low- (a) and (b) high-magnification cryoHAADF-STEM images of the cross sections of microbeads obtained by microtoming particles embedded in epoxy resin. The temperature of the sample holder during imaging was −100 °C. The accelerating voltage and emission current are 200 kV and 30 μA, respectively. Scale bar is 1 μm.

PTFEMA-rich layer (bright), PTFEMA−PS composite layer (gray) and PS layer (dark) to be ca. 95 ± 20, 120 ± 20, and 105 ± 10 nm, respectively.

To explain the formation of the composite phase between PS and PTFEMA layers, we refer to the difference in glass transition temperatures of PS and PTFEMA (100 and 60 °C, respectively).[22] At the temperature of polymerization of 80 °C, styrene diffused into the soft PTFEMA layer. This process was followed by phase separation of PS and PTFEMA, as shown in Figure 3b.

Characterization of the Composition of the Layers. We used energy-dispersive X-ray (EDX) analysis for elemental mapping of carbon and fluorine elements in the alternating layers of the microbeads. Polystyrene and PTFEMA layers have a different content of carbon and fluorine. On the basis of the molecular structure of these polymers, the content of carbon is 92.3 and 42.8 wt % in the PS and PTFEMA layers, respectively. The content of fluorine is 33.9 and 0 wt % in PTFEMA and in PS layers, respectively. Thus, we expected a sharp modulation in the content of carbon and fluorine in EDX spectra of the microtomed particles. Figure 4 shows the variation in carbon and fluorine contents in the different layers of the particles. The profiles were acquired for the same particle slice. When STEM examination was carried out at room temperature, we observed five peaks for carbon content, corresponding to the PS core and two PS layers (Figure 4a, top profile). The modulation in fluorine content (Figure 4a, bottom profile) was smeared off, which further proved the "contrast inversion" effect due to the etching of the PTFEMA phase. By contrast, when using a cryoSTEM sample holder at −100 °C, we reduced radiation-induced damage of the sample and obtained a sharp modulation of both carbon and fluorine contents. Figure 4b clearly demonstrates periodic variation in composition of the alternating layers of the polymer particles.

In summary, we demonstrated several important features of TEM imaging of multilayer polymer particles. These features include (a) contrast inversion in the composite microspheres imaged under high magnification due to the etching of the softer fluorinated phase, (b) "disappearance" of the outmost PS layer

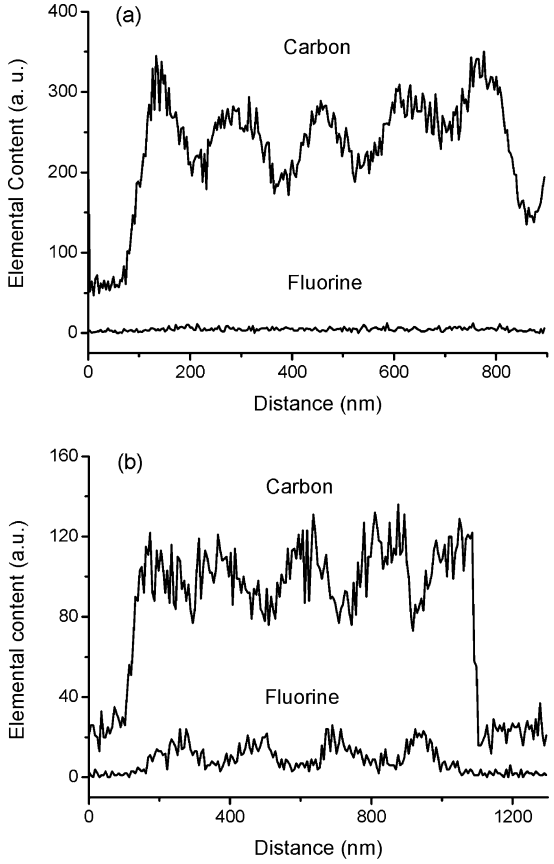

Figure 4. Variation in carbon and fluorine contents in multilayer particles measured by energy-dispersive X-ray analysis. The experiments were conducted for the same particle slice by using a sample holder at room temperature (a) and at −100 °C (b).

in the particles, caused by the mass−thickness match between PS and epoxy resin (most frequently used in TEM imaging), and (c) change in particle shape in the stage of cryomicrotoming due to a strong shear force imposed on the microbeads. These effects can lead to the incorrect conclusions about particle composition, structure, and shape. We showed that each of these artifacts can be avoided by conducting TEM imaging under appropriate conditions and/or by carrying out TEM imaging in complementary modes. We stress that contrast inversion is important in TEM studies of other polymer systems, e.g., in block copolymer systems where high-resolution imaging provides detailed information about polymer self-assembly.

Acknowledgment. The authors are grateful to NSERC for financial support of this work through the AGENO program. E.K. thanks Canada Research Chair support.

References and Notes

(1) Wang, G. J.; Kang, C. S.; Jin, R. G. *Prog. Org. Coat.* **2004**, *50*, 55−61.
(2) Kalinina, O.; Kumacheva, E. *Macromolecules* **2001**, *34*, 6380−6386.
(3) (a) Kumacheva, E.; Kalinina, O.; Lilge, L. *Adv. Mater.* **1999**, *11*, 231−234. (b) Siwick, B. J.; Kalinina, O.; Kumacheva, E.; Miller, R. J. D.; Noolandi, J. *J. Appl. Phys.* **2001**, *90*, 5328−5334.
(4) (a) Pham, H. H.; Gourevich, I.; Oh, J. K.; Jonkman, J. E.; Kumacheva, E. *Adv. Mater.* **2004**, *16*, 516−520. (b) Gourevich, I.; Pham, H.; Jonkman, J.; Kumacheva, E. *Chem. Mater.* **2004**, *16*, 1472−1479.
(5) (a) Brady, D.; Papen, G.; Sipe, J. E. *J. Opt. Soc. Am. B* **1993**, *10*, 644−657. (b) Alteheld, A.; Gourevich, I.; Field, L. M.; Paquet, C.; Kumacheva, E. *Macromolecules* **2005**, *38*, 3301−3306. (c) Gourevich, I.; Field, L. M.; Wei, Z.; Paquet, C.; Petukhova, A.; Alteheld, A.; Kumacheva, E.; Saarinen, J. J.; Sipe, J. E. *Macromolecules* **2006**, *39*, 1449−1454.
(6) Xu, X.; Asher, S. A. *J. Am. Chem. Soc.* **2004**, *126*, 7940−7945.

CDV

(7) (a) Cho, I.; Lee, K.-K. *J. Appl. Polym. Sci.* **1985**, *30*, 1903−1926. (b) Spiegel, S.; Landfester, K.; Lieser, G.; Boeffel, C.; Spied, H. W. *Macromol. Chem. Phys.* **1995**, *196*, 985−993.

(8) (a) Jönsson, J. E. L.; Hassander, H.; Jansson, L. H.; Törnell, B. *Macromolecules* **1991**, *24*, 126−131. (b) Jönsson, J. E. L.; Hassander, H.; Törnell, B. *Macromolecules* **1994**, *27*, 1932−1937.

(9) (a) Durant, Y. G.; Sundberg, E. J.; Sundberg, D. C. *Macromolecules* **1997**, *30*, 1028−1032. (b) Stubb, J.; Karlsson, O.; Jönsson, J. E.; Sundberg, E.; Durant, Y.; Sundberg, D. C. *Colloids Surf., A* **1999**, *153*, 255−270. (c) Ivarsson, L. E.; Karlsson, O. J.; Sundberg, D. C. *Macromol. Symp.* **2000**, *151*, 407−412.

(10) (a) Lee, S.; Rudin, A. *J. Polym. Sci., Part A: Polym Chem.* **1992**, *30*, 865−871. (b) Lee, C.-F.; Chiu, W. Y. *J. Appl. Polym. Sci.* **1997**, *65*, 425−438. (c) Kirsch, F.; Landfester, K.; Shaffer, O.; El-Aasser, M. S. *Acta Polym.* **1999**, *50*, 347−362.

(11) (a) Raghavan, D.; Gu, X.; Nguyen, T.; VanLandingham, M.; Karim, A. *Macromolecules* **2000**, *33*, 2573−2583. (b) Maye, M. M.; Luo, J.; Han, L.; Zhong, C. J. *Nano Lett.* **2001**, *1*, 575−579. (c) Sommer, F.; Duc, T. M.; Pirri, R.; Meunier, G.; Quet, C. *Langmuir* **1995**, *11*, 440−448.

(12) Rademann, J.; Barth, M.; Brock, R.; Egelhaaf, H.-J.; Jung, G. *Chem.*−*Eur. J.* **2001**, *7*, 3884−3889.

(13) (a) Koprinarov, I.; Hitchcock, A. P.; Li, W. H.; Heng, Y. M.; Stöver, H. D. H. *Macromolecules* **2001**, *34*, 4424−4429. (b) Takekoh, R.; Okubo, M.; Araki, T.; Stöver, H. D. H. *Macromolecules* **2005**, *38*, 542−551.

(14) (a) Landfester, K.; Boeffel, C.; Lambla, M.; Spiess, H. W. *Macromolecules* **1996**, *29*, 5972−5980. (b) Landfester, K.; Spiess, H. W. *Acta Polym.* **1998**, *49*, 451−464.

(15) (a) Hourston, D. J.; Song, M.; Pang, Y. J. *Braz. Chem. Soc.* **2001**, *12*, 87−92. (b) Hourston, D. J.; Zhang, H. X.; Song, M.; Pollock, H. M.; Hammiche, A. *Thermochim. Acta* **1997**, *194*, 23−31.

(16) Stubbs, J. M.; Sundberg, D. C. *Polymer* **2005**, *46*, 1125−1138.

(17) Brandrup, J.; Immergut, E. H.; Grulke, E. A. *Polymer Handbook*, 4th ed.; Wiley & Sons: New York, 1999.

(18) Koizumi, S.; Tadano, K.; Tanaka, Y.; Shimidzu, T.; Kutsmizu, S.; Yano, S. *Macromolecules* **1992**, *25*, 6563−6567.

(19) Sawyer, L. C.; Grubb, D. T. *Polymer Microscopy*; Springer: Berlin, 1995; p 57.

(20) Groves, T. *Ultramicroscopy* **1975**, *1*, 15−31.

(21) Fosythe, J. S.; Hill, D. J. T. *Prog. Polym. Sci.* **2000**, *25*, 101−136.

(22) Karlsson, L. E.; Karlsson, O. J.; Sundberg, D. C. *J. Appl. Polym. Chem.* **2003**, *90*, 905−915.

MA052029Z